Dalton Transactions

Accepted Manuscript

ROYAL SOCIETY OF CHEMISTRY

www.rsc.org/dalton

Journal Name

RSCPublishing

ARTICLE

Two series of reactants' ratio-dependent lanthanide organic frameworks derived from nicotinic acid N-oxide and oxalate: Synthesis, crystal structures and luminescence properties

Cite this: DOI: 10.1039/x0xx00000x

Received ooth January 2012,
Accepted ooth January 2012

DOI: 10.1039/x0xx00000x

www.rsc.org/

Yanyan Yu, Lijuan Zhang*, Yunshan Zhou* and Zareen Zuhra

Two series of lanthanide(III)–organic frameworks with the molecular formula $[Ln_2(NNO)_2(OX)_2(H_2O)_4]_n$ (Ln = Eu **1**, Tb **2**, Sm **3**, Dy **4**, Gd **5**) and $[Ln_2(NNO)_4(OX)(H_2O)_2]_n$ (Ln = Eu **6**, Tb **7**, Sm **8**, Dy **9**, Gd **10**) were synthesized successfully under same hydrothermal conditions with nicotinic N-oxide (HNNO) and oxalic acid (H_2OX) as the mixed ligands merely through varying the molar ratio of the reactants. The compounds were characterized by IR, elemental analysis, UV, TG-DTA and powder X-ray diffraction (XRD). X-ray single-crystal diffraction analyses of compounds **1** and **7** selected as representatives and powder XRD analysis of the compounds revealed that both of the two series of compounds feature three-dimensional (3-D) open frameworks, crystallize in triclinic *P*-1 space group while with different unit cell parameters. In compound **1**, pairs of Eu^{3+} ions and pairs of NNO^- ligands connect each other alternately to form a 1-D infinite Eu-NNO double chain, the adjacent 1-D double-chains are then joined together through OX^{2-} ligands leading to a 2D layer, the 2-D layers are further 'pillared' by OX^{2-} ligands resulting in a 3-D framework. In compound **7**, the 1-D Tb-NNO infinite chain and its 2-D layer are formed in almost similar fashion to that adopted in compound **1**. The difference between the structures of the two compounds **1** and **7** is that the adjacent 2-D layers in compound **7** are further connected by NNO^- ligands resulting in a 3-D framework. The photoluminescence properties and energy transfer mechanism of the compounds were studied systematically. The energy level of the lowest triplet states of the HNNO ligand (23148 cm^{-1}) was determined based on the phosphorescence spectrum of compound **5** at 77 K. The $^5D_0$ (Eu^{3+}) and $^5D_4$ (Tb^{3+}) emission lifetimes (0.46 ms, 0.83 ms, 0.69 ms and 0.89 ms) and overall quantum yields (1.03%, 3.29%, 2.58% and 3.78%) for the compounds **1**, **2**, **6** and **7**, respectively.

INTRODUCTION

In recent years, the rational design and assembly of photoluminescent lanthanide (III) metal-organic frameworks (Ln-MOFs), has been of considerable interest due to their intriguing topology, architectures and potential applications in fluorescent probe, light-emitting diodes, sensors and fluorescent labelling. Therefore the synthesis and design of novel Ln-MOFs is always the hot spot in the field of luminescence materials science for decades. Trivalent lanthanide ions such as Eu^{3+}, Tb^{3+}, Sm^{3+} and Dy^{3+} exhibit intense, long-lived, line-like and high monochromatic emission in the visible region due to the shielding of the 4f orbitals by the filled $^5S_2$ and $^5P_6$ subshells.[2] However, the lanthanide ions suffer from weak light absorption due to the forbidden f-f transitions, making the direct excitation of the metals very inefficient and difficult.[3] Such weak absorption problem can be overcome through introducing conjugate and rigid organic ligands as antennas to sensitize the luminescence of lanthanide ions by energy transfer from the ligand to lanthanide ion, such a process is known as "antenna effect".[4]

Thus, the key of design and synthesis of Ln-MOFs is to choose appropriate organic ligands with bridging functions and conjugate structures as the antenna ligands. As the lanthanide ion is oxygenphilic, organic carboxylic acid is a good choice for the construction of an abundant variety of multidimensional structures of Ln-MOFs.[3-5] Among organic carboxylic acids, nicotinic acid with N-heterocyclic rigid ring containing N- and O-donors and with conjugate structures are of particular use in building novel Ln-MOFs with excellent luminescent properties.[5] Compared with the parent ligand nicotinic acid, its derivative nicotinic acid N-oxide (HNNO) having an oxygen atom in place of nitrogen donor site can make it easier to get Ln-MOFs due to its increasing flexibility and coordination ability. Moreover, various organic dicarboxylic acids[1a, 6] are

often used to construct Ln-MOFs composed of mixed ligands with various structures and desiring luminescence properties.[7] Among them, oxalic acid with bridging function and the moderate length[8] acting as a linker in the design of Ln-MOFs not only can coordinate with lanthanide ions but also can replace solvent molecules to reduce the quenching effect of lanthanide ions.[9] Besides, oxalic acid can also participate in the process of intramolecular energy transfers, so it is a common ligand to construct Ln-MOFs.[1a, 6, 10]

Importantly, it is well known that many synthetic factors such as, the ratio of the reactants, solvents, reaction temperature, pH value, types of anions often affect the results in constructing the Ln-MOFs, so it is still a great challenge to control structures with desired luminescence properties due to intricate coordination geometry of the central lanthanide ions and coordination modes of organic ligands.[11] In order to investigated the influence of different synthetic factors on the structures of the Ln-MOFs and luminescent properties, in this work, both HNNO and H_2OX were selected as mixed ligands (Chart S1) to react with lanthanide ions Eu^{3+}, Tb^{3+}, Sm^{3+}, Dy^{3+} and Gd^{3+} under same hydrothermal conditions leading to two series of Ln-MOFs containing the mixed ligands merely through adjusting the molar ratio of the reactants: $[Ln_2(NNO)_2(OX)_2(H_2O)_4]_n$ (Ln = Eu **1**, Tb **2**, Sm **3**, Dy **4**, Gd **5**) and $[Ln_2(NNO)_4(OX)(H_2O)_2]_n$ (Ln = Eu **6**, Tb **7**, Sm **8**, Dy **9**, Gd **10**). Compounds **1** and **7** selected as a representative were structurally characterized. The luminescence properties and energy transfer mechanism of the compounds were studied systematically as well.

Experimental Section

Materials and Methods

All materials including solvents were obtained from commercial sources, were of reagent grade and were used without further purification. IR spectra were recorded on a Nicolet FTIR-170SX spectra photometer as KBr pellets in the range 4000–400 cm^{-1}. ^{13}C NMR spectra were recorded on a Bruker AV 400 spectrometer. Elemental analyses for C, H and N were performed on a Perkin-Elmer 240C analytical instrument, while Eu, Tb, Sm, Dy and Gd in all samples, which were dissolved in dilute hydrochloric acid, were carried out by using an ICPS-7500 model inductively coupled plasma emission spectrometer (ICP-ES). Thermogravimetric analyses were carried out on a NETZSCH STA 449C unit at a heating rate of 5℃/min under air. Powder X-ray diffraction (XRD) measurements were carried out on a Rigaku D/max 2500 X-ray diffractometer with a graphite-monochromatized Cu Kα line (λ= 0.15405 nm) as the incident beam. The scanning rate was set to 10 °/min in the 2θ range from 3 ° to 55 °. The excitation and emission spectra for the complexes in the solid state were measured on a Hitachi F-7000FL fluorescence spectrophotometer with both excitation and emission slits at 5 nm at room temperature. The scan speed is 1200 nm/min, and PMT voltage is 400 V. The phosphorescence spectra of compound **5** in solid state at 77K were measured with a Hitachi F-7000 FL fluorescence spectrophotometer with emission slit of 5 nm. The scan speed is 240 nm/min and PMT voltage is 600 V using a xenon arc lamp (150 W) as the light source. The luminescence decay curves and photoluminescence quantum yields of the samples were obtained using a FLS 980 Combined Fluorescence Lifetime and Steady State Spectrometer.

Preparation of Nicotinic acid N-oxide

Nicotinic acid N-oxide (HNNO) were prepared from nicotinic acid in the presence of acetic acid and hydrogen peroxide according to the literature,[12] and was checked by IR spectrum, elemental analysis and ^{13}C NMR. Anal. calcd for $C_6H_5NO_3$ (HNNO): C, 51.80; H, 3.62; N, 10.07. Found: C, 51.83; H, 3.53; N, 10.14%. IR(KBr, ν/cm^{-1}) 3430(m), 3074, 1716(m), 1570, 1483(m), 760(s), 1204(s), 1440(s), 933(s), 822(m). ^{13}C NMR (ppm): 164.2, 142.1, 138.9, 130.5, 126.7, 125.4 (Figure S1).

Synthesis of $[Eu_2(NNO)_2(OX)_2(H_2O)_4]_n$ 1

A mixture of HNNO (0.66 mmol, 0.0916 g), H_2OX (0.5 mmol, 0.0630 g), Eu_2O_3 (0.25 mmol, 0.088 g), H_2O (10 mL) was placed in a 25 mL Teflon-lined stainless steel veFig. sssel, was kept under autogenous pressure at 170 ºC for 3 days and slowly cooled to room temperature at the rate 10 ℃ per hour. Colorless block shape single crystals were mechanically collected under microscope after drying under vacuum at 20 ºC, with yield of 0.147g, 71.2% based on Eu. Anal. calcd (%) for $C_{16}H_{16}Eu_2N_2O_{18}$: C, 23.20; H, 1.95; N, 3.38; Eu, 36.40. Found: C, 23.10; H, 1.99; N, 3.43; Eu, 36.45. IR (KBr, ν/cm^{-1}) 3610(m), 1653(s), 1593(s), 1411(s), 1317(m), 1229(s), 1177(m), 1134(m), 1026(m), 951(s), 790(s), 675(m), 579(m).

Synthesis of $[Tb_2(NNO)_2(OX)_2(H_2O)_4]_n$ 2

The compound was synthesized in a similar process to that for compound **1**, except that Tb_4O_7 (0.125 mmol, 0.093 g) was used instead of Eu_2O_3. Colorless block shape crystals were obtained. Yield: 0.145 g, 68.9% based on Tb. Anal. calcd. (%) for $C_{16}H_{16}Tb_2N_2O_{18}$: C, 23.81; H, 1.92; N, 3.33; Tb, 37.74. Found: C, 22.79; H, 1.95; N, 3.30; Tb, 37.60. IR(KBr, ν/cm^{-1}) 3610(m), 1651(s), 1592(s), 1410(s), 1317(m), 1229(s), 1177(m), 1134(m), 1026(m), 951(s), 790(s), 675(m), 579(m).

Synthesis of $[Sm_2(NNO)_2(OX)_2(H_2O)_4]_n$ 3

The compound was synthesized in a similar process to that for compound **1**, except that Sm_2O_3 (0.25 mmol, 0.087 g) was used instead of Eu_2O_3. Yield: 0.153 g, 74.0% based on Sm. Anal. calcd (%) for $C_{16}H_{16}Sm_2N_2O_{18}$: C, 23.29; H, 1.95; N, 3.39; Sm, 36.46. Found: C, 23.25; H, 1.98; N, 3.42; Sm, 36.45. IR(KBr, ν/cm^{-1}) 3610(m), 1654(s), 1594(s), 1411(s), 1317(m),1230(s), 1177(m), 1134(m), 1026(m), 951(s), 790(s), 675(m), 579(m).

Synthesis of $[Dy_2(NNO)_2(OX)_2(H_2O)_4]_n$ 4

The compound was synthesized in a similar process to that for compound 1, except that Dy_2O_3 (0.25 mmol, 0.093 g) was used instead of Eu_2O_3. Yield: 0.139 g, 65.6% based on Dy. Anal. calcd (%) for $C_{16}H_{16}Dy_2N_2O_{18}$: C, 22.63; H, 1.90; N, 3.30; Dy:

38.27. Found: C, 22.63; H, 1.95; N, 3.36; Dy, 38.33. IR(KBr, ν/cm^{-1}) 3610(m), 1653(s), 1595(s), 1410(s), 1317(m), 1230(s), 1177(m), 1134(m), 1026(m), 951(s), 790(s), 675(m), 579(m).

Synthesis of $[Gd_2(NNO)_2(OX)_2(H_2O)_4]_n$ 5

The compound was synthesized in a similar process to that for compound **1**, except that Gd_2O_3 (0.25 mmol, 0.091 g) was used instead of Eu_2O_3. Yield: 0.155 g, 74.0% based on Gd. Anal. calcd (%) for $C_{16}H_{16}Gd_2N_2O_{18}$: C, 22.91; H, 1.92; N, 3.34; Gd, 37.50. Found: C, 22.36; H, 1.96; N, 3.41; Gd, 37.44. IR(KBr, ν/cm^{-1}) 3610(m), 1654(s), 1596(s), 1410(s), 1317(m), 1233(s), 1177(m), 1134(m), 1026(m), 951(s), 790(s), 675(m), 579(m).

Synthesis of $[Eu_2(NNO)_4(OX)(H_2O)_2]_n$ 6

A mixture of HNNO (1.0 mmol, 0.138 g), H_2OX (0.5 mmol, 0.0630 g), Eu_2O_3 (0.25 mmol, 0.088 g), H_2O (10 mL) was placed in a 25 mL Teflon-lined stainless steel vessel under stirring, was kept under autogenous pressure at 170 ºC for 3 days and slowly cooled to room temperature at the rate 10 ℃ per hour. 0.174 g colorless block shape single crystals were collected under microscope after drying under vacuum at 20 ºC, with yield of 71% based on Eu. Anal. calcd (%) for $C_{26}H_{20}Eu_2N_4O_{18}$: C, 31.85; H, 2.06; N, 5.72; Eu, 31.01. Found: C, 31.82; H, 2.10; N, 5.68; Eu, 31.05. IR(KBr, ν/cm^{-1}) 3406(m), 1671(s), 1621(s), 1593(s), 1569(s), 1484(w), 1420(s), 1393(m), 1315(m), 1234(s), 1135(m), 1120(m), 1023(m), 925(s), 792(s), 768(m), 670(m), 448(s).

Synthesis of $[Tb_2(NNO)_4(OX)(H_2O)_2]_n$ 7

The compound was synthesized in a similar process to that for compound **6**, except that Tb_4O_7 (0.125 mmol, 0.093 g) was used instead of Eu_2O_3. Colorless block shape crystals were obtained, Yield: 0.151g, *ca*. 66% based on Tb. Anal. calcd (%) for $C_{26}H_{20}Tb_2N_4O_{18}$: C, 31.41%; H, 2.03%; N, 5.64%; Tb, 31.89. Found: C, 31.46; H, 2.07; N, 5.64%; Tb, 31.96. IR(KBr, ν/cm^{-1}) 3406(m), 1671(s), 1621(s), 1593(s), 1569(s), 1484(w), 1420(s), 1393(m), 1315(m), 1234(s), 1135(m), 1120(m), 1023(m), 925(s), 792(s), 768(m), 670(m), 448(s).

Synthesis of $[Sm_2(NNO)_4(OX)(H_2O)_2]_n$ 8

The compound was synthesized in a similar process of that for compound **6**, except that Sm_2O_3 (0.25 mmol, 0.087 g) was used instead of Eu_2O_3. Yield: 0.166 g, 68.0% based on Sm. Anal. calcd (%) for $C_{26}H_{20}Sm_2N_4O_{18}$: C, 31.95; H, 2.06; N, 5.73; Sm, 30.78. Found: C, 31.90; H, 2.07; N, 5.73; Sm, 30.75. IR (KBr, ν/cm^{-1}) 3406(m), 1671(s), 1621(s), 1593(s), 1569(s), 1484(w), 1420(s), 1393(m), 1315(m), 1234(s), 1135(m), 1120(m), 1023(m), 925(s), 792(s), 768(m), 670(m), 448(s).

Synthesis of $[Dy_2(NNO)_4(OX)(H_2O)_2]_n$ 9

The compound was synthesized in a similar process of that for compound **6**, except that Dy_2O_3 (0.25 mmol, 0.093 g) was used instead of Eu_2O_3. Yield: 0.163 g, 65.0% based on Dy. Anal. calcd (%) for $C_{26}H_{20}Dy_2N_4O_{18}$: C, 31.18; H, 2.01; N, 5.60; Dy, 32.45. Found: C, 31.13; H, 2.05; N, 5.64; Dy, 32.37. IR (KBr, ν/cm^{-1}) 3406(m), 1671(s), 1621(s), 1593(s), 1569(s), 1484(w), 1420(s), 1393(m), 1315(m), 1234(s), 1135(m), 1120(m), 1023(m), 925(s), 792(s), 768(m), 670(m), 448(s).

Synthesis of $[Gd_2(NNO)_4(OX)(H_2O)_2]_n$ 10

The compound was synthesized in similar process of that for compound **6**, except that Gd_2O_3 (0.25 mmol, 0.091 g) was used instead of Eu_2O_3. Yield: 0.186 g, 75.0% based on Gd. Anal. calcd (%) for $C_{26}H_{20}Gd_2N_4O_{18}$: C, 31.51; H, 2.03; N, 5.65; Gd, 31.70. Found: C, 31.36; H, 1.96; N, 5.61; Gd, 31.75. IR (KBr, ν/cm^{-1}) 3406(m), 1671(s), 1621(s), 1593(s), 1569(s), 1484(w), 1420(s), 1393(m), 1315(m), 1234(s), 1135(m), 1120(m), 1023(m), 925(s), 792(s), 768(m), 670(m), 448(s).

X-ray Crystallography

Table 1. Crystal data and structure refinement for compounds **1** and **7**.

identification code	1	7
Empirical formula	$C_{16}H_{16}Eu_2N_2O_{18}$	$C_{26}H_{20}Tb_2N_4O_{18}$
Formula weight	828.23	994.30
Temperature	100(2) K	102.5 K
Wavelength	0.71073 Å	0.71073 Å
Crystal system	Triclinic	Triclinic
Space group	*P*-1	*P*-1
Unit cell dimensions	a = 6.6723(9) Å	a = 8.2954(4) Å
	b = 8.3982(13) Å	b = 9.7473(5) Å
	c = 10.312(2) Å	c = 9.8872(6) Å
	α = 75.470(16)°	α = 101.508(5)°
	β = 71.695(15)°	β = 108.666(5)°
	γ = 88.038(13)°	γ = 101.022(4)°
Volume	530.44(15) Å^3	713.62(7) Å^3
Z	1	1
Density(calculate)/Mg/m^3	2.593	2.314
Absorption coefficient/mm^{-1}	5.961	5.013
F(000)	396	478
Crystal size	0.34×0.35×0.30 mm^3	0.20×0.15×0.10 mm^3
2Θ range for data collection	3.22 to 26°	2.98 to 26°
Index ranges	-8 ≤ h ≤ 8, -10 ≤ k ≤ 10, -12 ≤ l ≤ 12	-10 ≤ h ≤ 10, -12 ≤ k ≤ 8, -12 ≤ l ≤ 11,
Reflections collection	3924	5412
Independent reflections	2084[R(int)=0.0345]	2800[R(int)=0.0424]
Goodness-of-fit on F^2	1.070	1.095
Final R indexes [I ≥ 2σ (I)]	R_1 = 0.0245, wR_2 = 0.0572	R_1 = 0.0273, wR_2 = 0.0637
Final R indexes [all data]	R_1 = 0.0262, wR_2 = 0.0579	R_1 = 0.0292, wR_2 = 0.0648
Largest diff. peak/hole / e Å^{-3}	0.779/-1.478	0.886/-1.579
CCDC No.	1020656	1023399

[a] $R_1 = \Sigma||F_o| - |F_c||/\Sigma|F_o|$. [b] $wR_2 = \Sigma[w(F_o^2 - F_c^2)^2]/\Sigma[w(F_o^2)^2]]^{1/2}$.

Crystallographic data of complexes **1** and **7** were collected at 100 K with an Oxford Diffraction Xcalibur Eos Gemini diffractometer with Mo Kα radiation (λ = 0.71073 Å) in the ω scans mode. The structure was solved by direct methods and refined on F^2 by full-matrix least-squares using SHELXTL-97 program package. All of the non-H atoms were refined with anisotropic displacement coefficients.[13] H atoms were added to a model in their geometrically ideal positions.[14] The crystal system of compounds **1** and **7** is triclinic and space group is *P*-1. Crystallographic data and experimental details for structural

analyses are summarized in Table 1 and the selected bond lengths and bond angles of compounds **1** and **7** are listed in Tables S1 and S2.

RESULTS AND DISCUSSION

Synthesis

Effect of the molar ratio of the reactants HNNO: H_2OX: lanthanide oxide on resultant structures of the synthesized compounds was investigated under the same hydrothermal reaction conditions. The results indicated that two series of Ln-MOFs were obtained under different molar ratios of the reactants: $[Ln_2(NNO)_2(OX)_2(H_2O)_4]_n$ (Ln = Eu **1**, Tb **2**, Sm **3**, Dy **4**, Gd **5**) and $[Ln_2(NNO)_4(OX)(H_2O)_2]_n$ (Ln = Eu **6**, Tb **7**, Sm **8**, Dy **9**, Gd **10**). When the molar ratio of the reactants lanthanide oxide: H_2OX: HNNO is 0.25: 0.5: 0.66, compounds **1** - **5** can be harvested. While compounds **6** - **10** can be obtained by changing the molar ratio of the reactants lanthanide oxide: H_2OX: HNNO to 0.25: 0.5: 1.0. When the dosage of HNNO is in the range of 0.66 mmol ~ 1 mmol, the mixture of the two series of compounds can be acquired (Scheme 1). It should be noted that compound **6** was synthesized successfully, structurally characterized and reported in our previous work.[10a] In this work, compounds **6** - **10** were synthesized according to the same method with the published method in order to compare the structural differences with compounds **1** - **5** and investigate the relationship between the structures and luminescence properties of the compounds.

Scheme 1. The schematic diagram of synthesis compounds **1**-**10** (Ln = Eu, Sm, Dy and Gd, *x* = 2, *y* = 3; Ln = Td, *x* = 4, *y* = 7)

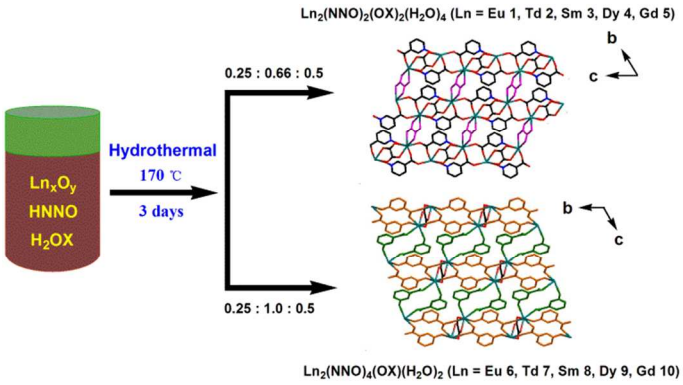

IR spectra of the free ligand and compounds 1−10

The IR spectra of compounds **1** - **10** and the free ligand HNNO are shown in Fig. 1. In the IR spectrum of HNNO, a broad band in range of 2200 - 3000 centered at 2500 cm^{-1} can be assigned to O−H stretching vibrations of the carboxylic groups.[15] The strong band at 3074 cm^{-1} can be attributed to the C−H stretching vibrations of the pyridine rings.[16] The strong band centered at 1716 cm^{-1} arises from the stretching vibrations of the C=O bond from carboxylic groups of the ligand.[17] Two bands at 1570 and 1483 cm^{-1} can be assigned to the stretching vibrations of the C=N bond of pyridine ring and one strong band at 1440 cm^{-1} is due to the characteristic vibration frequency of the pyridine ring.[18] Furthermore, the band at 1204 cm^{-1} is from the stretching vibrations of the N-O group.[19]

The IR spectra of compounds **2**, **3**, **4** and **5** are analogous to that of compound **1**, implying their isomorphous nature, so compound **1** was selected as the representative to discuss here. In the IR spectrum of compound **1**, the N-O stretching vibration appearing at 1228 cm^{-1} indicates that O atom of N-O bond coordinates with Eu^{3+} ion.[20] Two bands at 1446 cm^{-1} and 1653 cm^{-1} can be assigned to symmetric stretching and asymmetric of carboxylate group implying that the carboxylic group of HNNO ligand is deprotonated and coordinate with Eu^{3+} ions,[21] which is consistent with the following X-ray single-crystal structure analysis of the compound **1**.

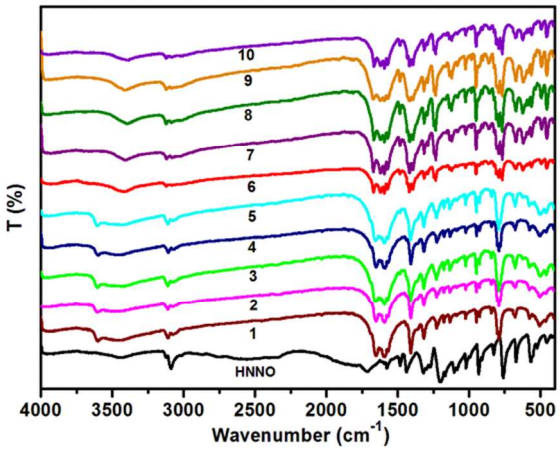

Fig. 1 IR spectra of nicotinic acid N-oxide and the compounds of **1**-**10**

The IR spectra of compounds **6** - **10** are almost the same, similarly, the compound **6** was chosen as the representative to discuss here. Four peaks at 1420(s), 1393(s), 1593(s), 1569(s) cm^{-1} can be assigned to symmetric and asymmetric stretching of carboxylate groups of the ligands, and the peak at 1224 cm^{-1} assigned to the N-O stretching vibration indicated that carboxylic groups are deprotonated and coordinate with Eu^{3+} ion and O atom of N-O bond coordinates with Eu^{3+} ion.[20, 21]

The IR spectra of compounds **6** - **10** are similar to that of compounds **1** - **5**, but some differences can be found, which are caused by the different number and different coordination modes of ligands in the two series of compounds.

Powder XRD patterns

Powder X-ray diffraction experiments were carried out for compounds **1** - **10**. The experimental PXRD patterns of compounds **1** - **5** with the simulated pattern of compound **1** and compounds **6** - **10** with the simulated pattern of compound **7** are shown in Fig. 2 and Fig. 3, respectively. The powder XRD patterns for the as-obtained bulk materials of compounds **1** - **5** and **6** - **10** closely match the simulated ones indicating that the phases of the final resulting compounds **1** - **5** and **6** - **10** are pure solid-state phases, no further by-product in the collected products was found, and compounds **1** - **5** and **6** - **10** are isomorphous, respectively.

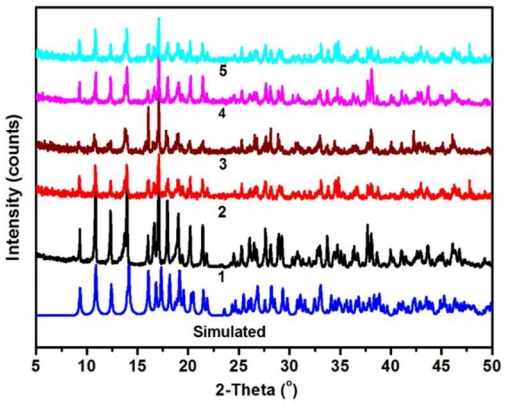

Fig. 2 The powder X-ray diffraction patterns of compounds **1**-**5** and the simulated for compound**1**

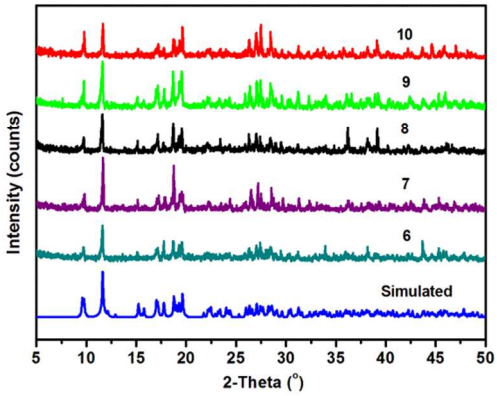

Fig. 3 The powder X-ray diffraction patterns of compounds **6**-**10** and the simulated for compound **7**

Description of the structures of the compounds 1-10

According to the results of powder X-ray diffraction analysis, the compounds **1-5**, namely $[Ln_2(C_6H_4NO_3)_2(C_2O_4)_2(H_2O)_4]_n$ (Ln = Eu **1**, Tb **2**, Sm **3**, Dy **4**, Gd **5**) are isostructural, which are crystallized in triclinic crystal system with *P*-1 space group. So, as a representative, the structure of compound **1** was determined by single crystal X-ray diffraction analysis.

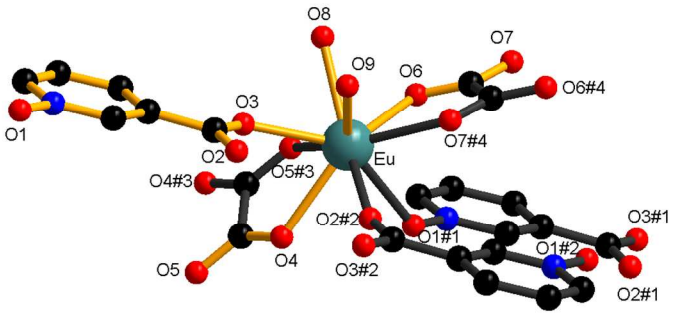

Fig. 4 Local coordination environment of Eu^{3+} ion in **1** (Atoms composing the asymmetric unit of each material are connected by yellow-filled bonds, H atoms were omitted for clarity). Symmetry code: (#1) +x, +y, 1+z; (#2) 1-x, 1-y, 1 -z; (#3) 1-x, 2-y, 1-z; (#4) -x, 1-y, 2-z.

As shown in Fig. 4, the asymmetric unit of compound **1** contains one crystallographically independent Eu^{3+} ion, one NNO^- ligand, one OX^{2-} ligand and two coordinated water molecules. Each Eu^{3+} ion is nine-coordinate with nine oxygen atoms from three individual NNO^- ligands (O3, O2#2, O1#1), two OX^{2-}(O6, O7#4, O4, O5#3), and two coordinated water molecules (O8, O9), forming a distored tricapped trigonal prism (Fig. S2a). The Eu−O bond lengths are in the range of 2.3549(33) − 2.5299(38) Å, and the O−Eu−O bond angles are in the range of 65.614(108)−141.744(108)°, which are similar to those in the reported Eu complexes.[1a,1c]

In compound **1**, as illustrated in Fig. 5(a), the NNO^- ligand adopts only one coordination mode: the carboxylate groups adopt μ_2-η^1-η^1 coordination mode linking two Eu^{3+} ions and its N-oxide moiety linking one Eu^{3+} ion, while each oxalate links two Eu^{3+} ions (Figure 5(c)).

The 3-D framework of compound **1** can be described as follows: two Eu^{3+} ions are bridged by a pair of NNO^- ligands (mode Fig. 5(a)) by their carboxylic groups, forming a 1D double infinite chain along *c* direction, in which the neighbouring Eu···Eu distance is *ca*. 10.3 Å (Fig. 6(a)). Then, the adjacent 1-D double chains are linked by OX^{2-} ligands (mode Fig. 5(c)) forming a 2D wavelike layer in *ac* plane with the shortest interchain Eu···Eu distance being *ca*. 6.3 Å (Fig. 6(b)) which is approximately equal to the bridging OX^{2-} length. The adjacent 2-D layers are further 'pillared' by OX^{2-} ligands (mode Figure 5(c)) resulting in a 3-D open framework with pseudo-1-D channels (Fig. 6(c)), in which the shortest interlayer Eu···Eu distance is *ca*. 6.3 Å. Although compound **1** exhibits an interesting 3-D framework structure, no solvent accessible void can be calculated by the CALC SOLV command in PLATON.[22] The Vander Waals radii of the constituent atoms are responsible for the compact framework structure.

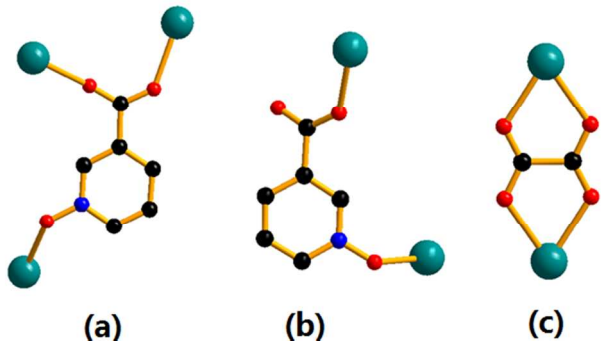

Fig. 5 Coordination modes for NNO- and OX^{2-} adopted in compounds **1** and **7**

In order to better understand the 3-D open framework of compound **1**, topological analysis of compound **1** was carried out. Each Eu^{3+} ion links five ligands (two OX^{2-} ligands and three NNO^- ligands) and therefore is regarded as a pentacorner-share holder and each NNO^- ligand links three Eu^{3+} ions and it is regarded as a tricorner-share holder; each OX^{2-} ligand links two Eu^{3+} ions and is regarded as a bicorner-share holder. As shown in Fig. 6d, the connectivity of these holders in

compound **1** results in the 3-D framework featuring a binodal (3,5)-connected net with Point (Schläfli) symbol of $(4^2\cdot6^5\cdot8^3)(4^2\cdot6)$.

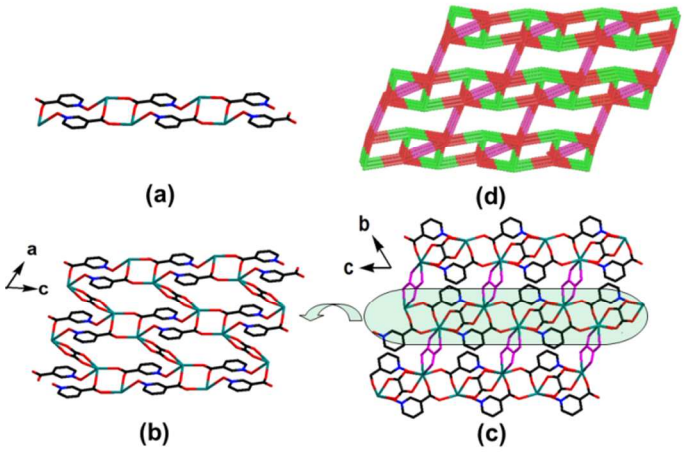

Fig. 6(a) The 1-D Eu-NNO double chain along *c* direction in compound **1**; (b) the 2-D layer composed of the 1-D double chains in *ac* plane in compound **1**; (c) the 3-D open framework structure composed of 2-D layers in compound **1** (Colour code: C in pyridine, black; C in oxalate, black and red; Eu, tea; N, blue; O, red); (d) topology along *a* direction in compound **1** (red node: Eu^{3+} ion; green node: NNO^-; purple node: OX^{2-}). All H atoms were omitted for clarity.

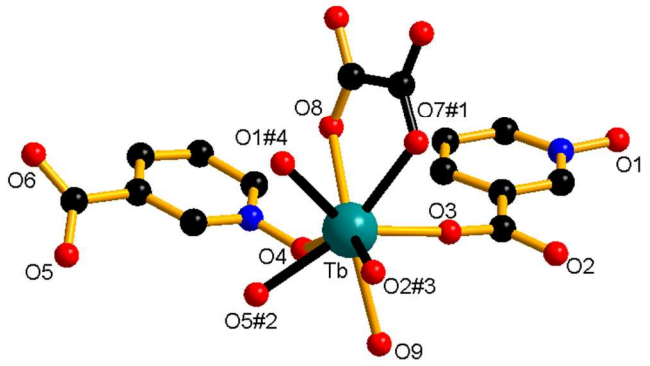

Fig. 7 Local coordination environment of Tb^{3+} ion in **7** (Atoms composing the asymmetric unit of each material are connected by yellow-filled bonds, H atoms were omitted for clarity). Symmetry code: (#1) +x, 1+y, z; (#2)1-*x*, 1-*y*, -*z*; (#3) 1-*x*, 1-*y*, 1-*z*; (#4) 2-x, 2-y, 1-z; (#5) x, y-1, z.

Single-crystal X-ray diffraction analysis revealed that compound **7** crystallizes in the triclinic *P*-1 space group. The asymmetric unit contains one crystallographically independent Tb^{3+} ion, two NNO^- ligands, half OX^{2-} and one coordinated water molecule (Fig. 7), each Tb^{3+} ion is eight-coordinate with eight oxygen atoms from five individual NNO^- ligands (O1#4, O2#3, O3, O4, O5#2), one coordinated OX^{2-}(O7#1, O8), and one water molecule (O9), forming a distorted bicapped trigonal prism (Fig. S2b) The Tb–O bond lengths are in the range of 2.3479 (6) Å − 2.4536 (7) Å, and the O–Tb–O bond angles are in the range of 66.803 (13)° − 147.492 (18)°, which are similar to those in the reported Tb complexes.

The 3-D framework of compound **7** can be described as the follows: two Tb^{3+} ions are bridged by a pair of NNO^- ligands (mode Fig. 5(a)) through their carboxylic groups forming a 1-D double chain along *b* direction, in which the neighbouring Tb⋯Tb distance is *ca*. 9.75 Å (Fig. 8(a)). Then, the neighbouring 1-D double chains are linked by OX^{2-} ligands (mode Fig. 5(c)) forming a 2D wavelike layer in *ab* plane with the shortest Tb⋯Tb distance is *ca*. 4.91 Å (Fig. 8(b)). The adjacent 2-D layers are further linked through NNO^- ligands with its one oxygen atom of the carboxylate linking one Tb^{3+} ion and its N-oxide moiety linking one Tb^{3+} ion (mode Fig. 5(b)), resulting in a 3-D open framework (Fig. 8(c)), in which the shortest interlayer Tb⋯Tb distance is *ca*. 7.91 Å. Although compound **7** exhibits an interesting 3-D framework structure, no solvent accessible void has been calculated from the CALC SOLV command in PLATON.[21]

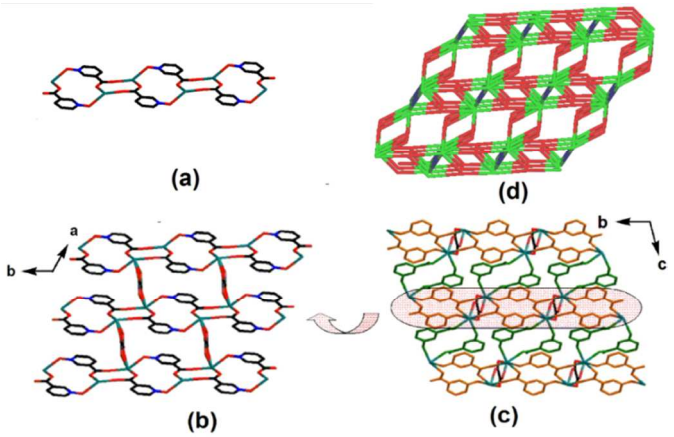

Fig. 8(a) The 1-D Tb-NNO double chain along *b* direction in compound **7**; (b) the 2-D layer composed of the 1-D Tb-NNO double chains in *ab* plane in compound **7**; (c) the 3-D open framework structure composed of 2-D layers in compound **7** (Colour code: C in pyridine, black and yellow; C in oxalate, black; Tb, tea; N, blue; O, red); (d) topology along *a* direction in compound **7** (green node: Tb^{3+} ion; red node: NNO^-; blue node: OX^{2-}). All H atoms were omitted for clarity.

Topological analysis on the 3-D structure of compound **7** was carried out. Each Tb^{3+} ion links six ligands (one OX^{2-} ligands and five NNO^- ligands) and therefore is regarded as a hexacorner-share holder and the two kinds of NNO^- ligands link two or three Tb^{3+} ions and are regarded as bicorner-share holder or tricorner-share holder, respectively. Each OX^{2-} ligands links two Tb^{3+} ions and is regarded as a bicorner-share holder. As shown in Fig. 8(d), the connectivity of these holders in compound **7** results in the 3-D framework featuring a binodal (3, 5)-connected net with Point (Schläfli) symbol of $(4^2\cdot6^5\cdot8^3)(4^2\cdot6)$.

Comparison of the structures of compound **1** with compound **7** reveals that both of them consist of Ln-NNO-OX 2-D layers composed of Ln-NNO double chains. The difference in their 3D construction lies in the different linkers connecting the adjacent 2-D layers. The adjacent 2-D layers in compound **1** are joined together via OX^{2-} ligands as linkers, while the adjacent 2-D layers in compound **7** are joined together via NNO^- ligands as linkers. Since all the compound were synthesized under the same hydrothermal conditions, except the molar ratio of the reactants HNNO: H_2OX: Ln_2O_3, the observed difference in the structures can only be attributed to the molar ratio of the

reactants , in other word, simply varying the molar ratio of the reactants can be adopted to produce different compounds of different properties.

Thermal stability analysis

In order to investigate the thermal stability of compounds **1** - **10**, TG-DTA experiments were performed, under flowing air in the temperature range of 30 to 850℃, for the compounds **1** and **3** selected as representatives of the compounds with formula $[Ln_2(NNO)_2(OX)_2(H_2O)_4]_n$ (Figure 9(a) and Figure 9(b)) and for the compounds **6** and **8** selected as representatives of the compounds with formula $[Ln_2(NNO)_4(OX)(H_2O)_2]_n$. Compounds **1** and **3** show good thermal stability from room temperature to 150 ºC for compound **1** and 140 ºC for compound **3**. The first weight loss of 8.62% (calcd 8.70%) for compound **1** and 8.34% (calcd 8.73%) for compound **3** in range of 150 to 175 ºC for compound **1** and 145 ºC to 173 ºC for compound **3** is endothermic process, corresponding to the loss of coordinated water molecules. Then the compounds show remarkable thermally stability again in range of 170 to 355 ºC for compound **1** and 173 ºC to 360 ºC for **3**. From 355 ºC to 650 ºC for compound **1** and 360 ºC to 740 ºC for compound **3**, the compounds get decomposed and lose organic parts with an exothermic process. The weight of the remaining residue (calc. 42.50%, found 42.99% for compound **1**; calc. 42.27%, found 42.36% for compound **2**) matches nicely the composition of Eu_2O_3 and Sm_2O_3, respectively.

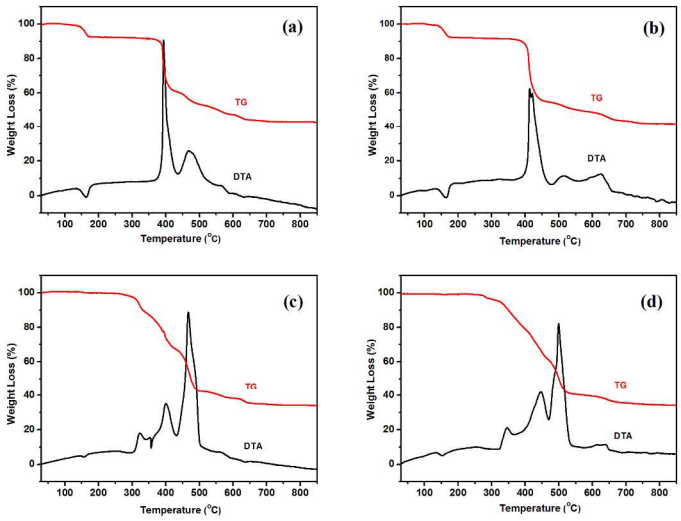

Fig. 9 TG-DTA curve of compound **1** (a), **3** (b), **6** (c) and **8** (d).

The compounds **6** and **8** are selected as representatives of the compounds with $[Ln_2(NNO)_4(OX)(H_2O)_2]_n$ to investigate their thermal stability (Fig. 9c and Fig. 9d). Compounds **6** and **8** both show remarkable thermal stability from room temperature to 300 ºC. Weight losses of 64.26% (calc. 64.09%) for compound **6** from 300 to 674 ºC and 64.25% (calc. 64.31%) for compound **8** from 300 to 670 ºC is exothermic process, corresponding to decomposition of the compounds and loss of coordinated water molecules and organic moieties. The weight of the remaining residue (calc. 35.91%, found 35.74% for compound **6**; calc. 35.69%, found 35.70% for compound **8**) matches nicely the composition of Eu_2O_3 and Sm_2O_3, respectively.

UV−vis absorption spectrum of HNNO

As shown in Fig. S3, the UV−Vis absorption spectrum of HNNO in DMF (c = 1×10^{-4} mol/L) shows one UV−Vis absorption band at 309 nm, which is assigned to the π→π* transition of the ligand.[23] The molar extinction coefficient value of the ligand at 309 nm is 6.88×10^3 L·mol^{-1}·cm^{-1} implying that the ligand is a good light-harvesting chromophore to sensitize lanthanide luminescence.[24] The singlet-state energy level can be calculated about 28653 cm^{-1} from the UV−Vis absorption spectrum absorbance edge of HNNO.

Diffuse Reflectance Spectroscopy

As shown in Fig. 10, the free ligands H_2OX and HNNO show absorption bands at 289 and 309 nm, which are assigned to the π→π* transition of the ligands.[23] The UV-vis spectra of compounds **1** - **5** and compounds **6** - **10** (Figure 10) are similar to the ligands indicating that the Ln^{3+} ions do not affect remarkably the singlet excited state of the free ligands.[25] While as compared with the free ligands HNNO and H_2OX, there are small blue shifts or red shifts in the Uv-vis spectra of the compounds, which indicates perturbation induced by the metal coordination or an effective interaction between the lanthanide cations and the organic ligands.[26]

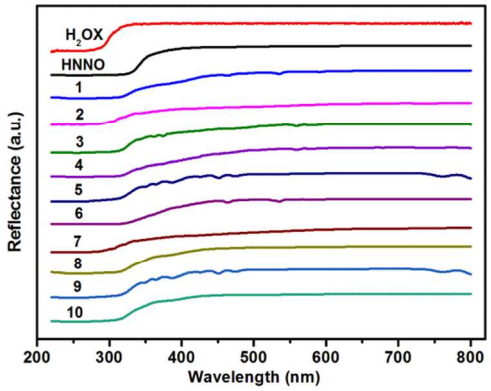

Fig. 10 Solid-state diffuse reflectance spectra of the free ligands and compounds **1-10**

Phosphorescence spectrum of compound 5

Since the lowest excited state $^6P_{7/2}$ of Gd^{3+} ion is too high to accept energy from a ligand, the triplet energy level of the corresponding ligand can be obtained from the phosphorescence spectrum of its Gd^{3+} complex at 77K.[27] As shown in Fig. S4, in the phosphorescence spectrum of compound **5**, two phosphorescence bands, peaking around 401 and 432 nm can be observed. As it is known that the triplet at 24570 cm^{-1} (401 nm) is attributed to the H_2OX ligand,[28] therefore the lowest triplet energy level of HNNO can be calculated about 23148 cm^{-1} (432 nm).

Energy transfer mechanism

According to Reinhoudt theory,[23] the intersystem crossing process becomes effective when $\Delta E(^1\pi\pi^*-^3\pi\pi^*)$ of a ligand is at least 5000 cm^{-1}. The calculated energy gap between the $^1\pi\pi^*$(28653 cm^{-1}) and $^3\pi\pi^*$(23148 cm^{-1}) levels being 5505 cm^{-1} for HNNO indicates effective intersystem crossing process in compounds **1** – **10** (Table 2).

Table 2 The singlet and triplet energy levels of HNNO ligand and energy level differences between Ln^{3+} ions and HNNO ligand in the complexes **1 - 4** and **6 - 9**.

Ligand	$^1\pi\pi^*$/ cm^{-1}	$^3\pi\pi^*$/ cm^{-1}	$\Delta E(^1\pi\pi^* - ^3\pi\pi^*)$/ cm^{-1}	$\Delta E(^3\pi\pi^* - ^5D_0)$/ cm^{-1}	$\Delta E(^3\pi\pi^* - ^5D_4)$/ cm^{-1}	$\Delta E(^3\pi\pi^* - ^4G_{5/2})$/ cm^{-1}	$\Delta E(^3\pi\pi^* - ^4F_{9/2})$/ cm^{-1}
HNNO	28653	23148	5505	5648	2648	5248	2272
H_2OX	38461	23923	14538	6423	3423	6670	3695

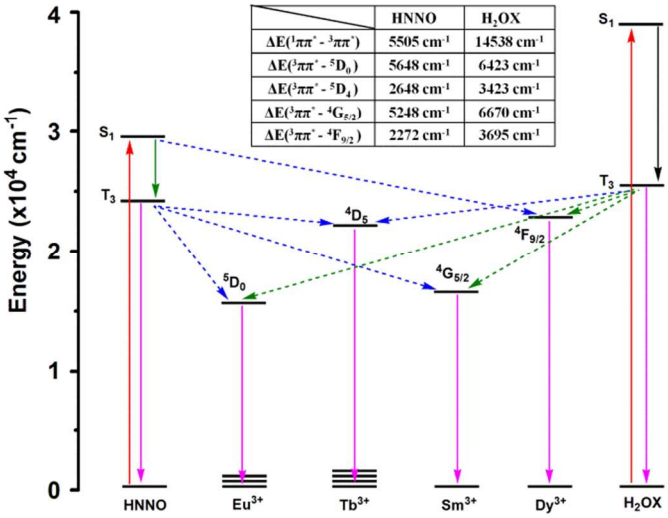

Fig. 11 Schematic energy level diagram and the energy transfer process in compounds **1 - 4** and **6 - 9**.

According to intramolecular energy transfer mechanism reported by Latva,[29] the energy difference between the lowest triplet level of a ligand and the resonant energy level of the Ln^{3+} ion plays a decisive role in energy transfer process in lanthanide complexes. An optimal value of the energy difference is assumed to exist around 3000 ± 500 cm^{-1} for Eu^{3+} ion and 2500 – 4500 cm^{-1} for Tb^{3+} ion,[30] the larger or smaller energy difference may result in a decrease of photoluminescence intensities of the lanthanide complexes.[5,31.]

As listed in Table 2, the energy difference between the lowest triplet levels of HNNO ligand and the resonant energy level of the Tb^{3+} ion ($^5D_4$, 20500 cm^{-1}) is 2648 cm^{-1}, which is within the optimal energy gap implying that the transitions from the triplet energy level of HNNO to Tb^{3+} ion is effective. However energy differences between the lowest triplet level of HNNO and the resonant energy levels of Eu^{3+} ion ($^5D_0$, 17500 cm^{-1}) , Sm^{3+} ion ($^4G_{5/2}$, 17900 cm^{-1}) and Dy^{3+} ions ($F_{9/2}$, 20875 cm^{-1}) are 5648 cm^{-1}, 5248 cm^{-1} and 2272 cm^{-1}, respectively which are all outside the optimal energy gap, indicating that the transitions from the triplet energy level of HNNO to Eu^{3+} ion, Sm^{3+} ion and Dy^{3+} ion are not effective. The lowest triplet level of oxalic acid is 24570 cm^{-1},[28] the energy difference between the lowest triplet of H_2OX and Eu^{3+} ion ($^5D_0$, 17500 cm^{-1}), Tb^{3+} ion ($^5D_4$, 20500 cm^{-1}), Sm^{3+} ion ($^4G_{5/2}$, 17900 cm^{-1}) and Dy^{3+} ion ($F_{9/2}$, 20875 cm^{-1}) are 6423, 3423, 6670 and 3695 cm^{-1}, respectively, which indicates that H_2OX is a suitable sensitizer for the luminescence of Tb^{3+} rather than Eu^{3+} ion, Sm^{3+} ion and Dy^{3+} ion. Thus, among the compounds **1** - **10**, it is predicted that compounds **2** and **7** can emit strong green characteristic luminescence of Tb^{3+} ion. Schematic energy level diagram and the energy transfer process in compounds **1** - **4** and compounds **6** - **9** are shown in Fig. 11.

Photoluminescence Properties

The solid-state photoluminescence spectra recorded at room temperature for compounds **1** and **6** are depicted in Fig. 12. The excitation spectra (Figure 12a) was monitored by the intense characteristic emission $^5D_0 \rightarrow ^7F_1$ (617 nm for compound **1** and 619 nm for compound **6**) of Eu^{3+} ion. A strong broad band with peaks at 284 nm and 315 nm can be attributed to the electronic transitions of the ligands. The weaker intensities of 4f–4f transitions of Eu^{3+} ions at 361 nm ($^7F_0 \rightarrow ^5D_4$), 380 nm ($^7F_0 \rightarrow ^5G_2$) and 393 nm($^7F_0 \rightarrow ^5L_6$) can be observed in the excitation spectra of compounds **1** and **6** indicating a more effective luminescence sensitization via the ligands.[27]

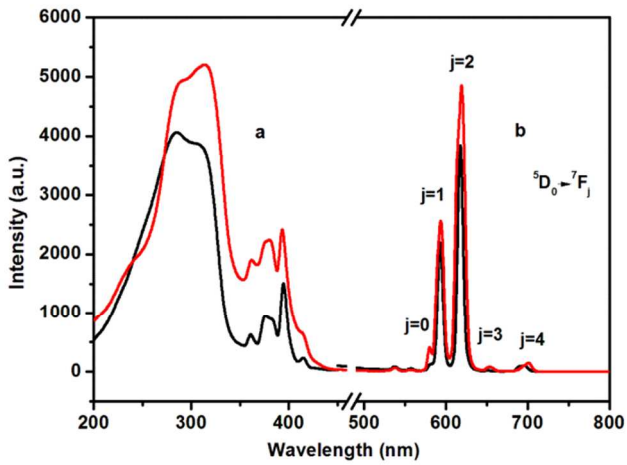

Fig. 12 The solid-state excitation spectra (a) and emission spectra (b) of compound **1** (black) (λ_{em} = 617 nm, λ_{ex} = 284 nm) and compound **6** (red) (λ_{em} = 619 nm, λ_{ex} = 315 nm)

The emission spectra (Fig. 12b) of compounds **1** and **6** monitored by 284 nm and 315 nm respectively exhibit the Eu^{3+} ion characteristic sharp bands assigned to $^5D_0 \rightarrow ^7F_j$ (j = 0 - 4) transitions of the Eu^{3+} ion: $^5D_0 \rightarrow ^7F_0$ (579 nm), $^5D_0 \rightarrow ^7F_1$ (593 nm), $^5D_0 \rightarrow ^7F_2$ (615 nm), $^5D_0 \rightarrow ^7F_3$ (653 nm) and $^5D_0 \rightarrow ^7F_4$ (697 nm).[31] The absence of bands from the higher excited states such as $^5D_1$ in the emission spectra implies that the nonradiative relaxation to the $^5D_0$ level is efficient.[32] The intensity of electric dipole transition ($^5D_0 \rightarrow ^7F_2$) is the strongest implying intense red luminescence.[33] The intensity ratio of 1.75 and 1.88 of $I(^5D_0 \rightarrow ^7F_2)/I(^5D_0 \rightarrow ^7F_1)$ indicates that the coordination

environment of Eu^{3+} ions in compounds **1** and **6** is lack of inversion center. [34] In addition, the $^5D_0 \rightarrow {}^7F_0$ transition of Eu^{3+} ion induced by crystal field J mixing is present in the emission spectra, which is only allowed for the 10 symmetries, C_s, C_1, C_2, C_3, C_4, C_6, C_{2v}, C_{3v}, C_{4v} and C_{6v} according to the ED selection rule.[35] In fact, the compounds **1** and **6** belongs to triclinic, Eu^{3+} ions occupy low symmetry crystal field belonging to C_1.[35]

The solid-state photoluminescence spectra of compounds **2** and **7** recorded at room temperature are depicted in Figure 13. The excitation spectra of compounds **2** and **7** (Fig. 13a) are monitored by the intense characteristic emission $^5D_4 \rightarrow {}^7F_5$ (544 nm for compound **2** and 545 nm for compound **7**) of Tb^{3+} ion, display a notable broad band with peaks at 287 nm and 320 nm in the range from 200 to 350 nm attributed to the electronic transitions of the ligands. The quite weak intensities of 4f−4f transitions of Tb^{3+} ion appearing in the excitation spectra of compounds **2** and **7** indicating a more effective luminescence sensitization via the ligand excited states than that of the direct intra $4f^8$ excitation.[26] The emission spectra (Fig. 12b) of compounds **2** and **7** measured upon excitation at the maximum excitation wavelength (288 nm for compound **2** and 320 nm for compound **7**) show the characteristic transitions $^5D_4 \rightarrow {}^7F_j$ (j = 3 - 6) of Tb^{3+} ions, viz., $^5D_4 \rightarrow {}^7F_6$(490 nm), $^5D_4 \rightarrow {}^7F_5$(544 nm), $^5D_4 \rightarrow {}^7F_4$(584 nm) and $^5D_4 \rightarrow {}^7F_3$(620 nm). The $^5D_4 \rightarrow {}^7F_5$ transition at 545 nm is the strongest emission, implying intense green luminescence.

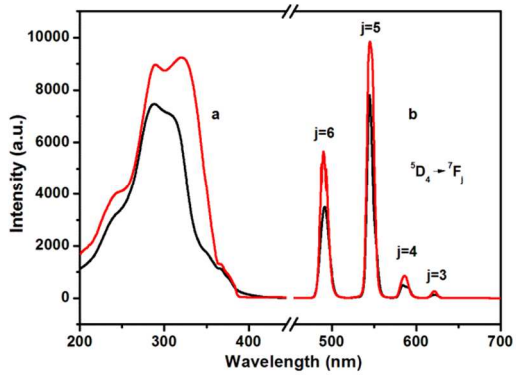

Fig. 13 The solid-state excitation (a) and emission spectra (b) of compound **2** (black) (λ_{ex} = 288 nm, λ_{em} = 545 nm) and **7** (red) (λ_{ex} = 320 nm, λ_{em} = 545 nm) .

The luminescence of compounds **3**, **4**, **8** and **9** are too weak to monitor which is mainly due to energy differences between the lowest triplet levels of the ligands and the resonant energy levels of Sm^{3+} and Dy^{3+} ions are outside the optimum value and thus the ligands cannot effectively sensitize Sm^{3+} and Dy^{3+} luminescence.

Interestingly, it is found that the emission intensities of compounds **6** and **7** are generally stronger than that of compounds **1** and **2** (Fig. 12 and Fig. 13), which can be explained by the following two reasons: First, there are two OX^{2-} and three NNO^- ligands coordinated with Ln^{3+} ions in compounds **1** and **2**, while in compounds **6** and **7**, there are one OX^{2-} and five NNO^- ligands coordinate with Ln^{3+} ions, i.e., there are more NNO^- ligands coordinating with Ln^{3+} ion and they can transfer energy to Ln^{3+} ion more effectively to sensitize Ln^{3+} luminescence in compounds **6** and **7** than that in compounds **1** and **2** (Table 3); second, in compounds **6** and **7**, the number of coordination water molecules is less than that in compounds **1** and **2**, so the quenching effects of Ln^{3+} ion caused by coordination interaction between coordination water molecules and Ln^{3+} ions was reduced.[33a, 36]

Table 3 Radiative lifetimes (τ_R), intrinsic quantum yields of the lanthanide luminescence step (Φ_{Ln}), sensitization efficiencies (η_{sens}), the experimentally determined luminescence lifetimes (τ_{obs}) and overall quantum yields (Φ_{tot}) of compounds **1**, **2**, **6** and **7**.

Compound	τ_R /ms	τ_{obs}/ms	Φ_{Ln} /(%)	η_{sens}/(%)	Φ_{tot} /(%)
1	6.90	0.46	6.60	15.61	1.03
2		0.83			3.29
6	6.25	0.69	11.04	23.37	2.58
7		0.89			3.78

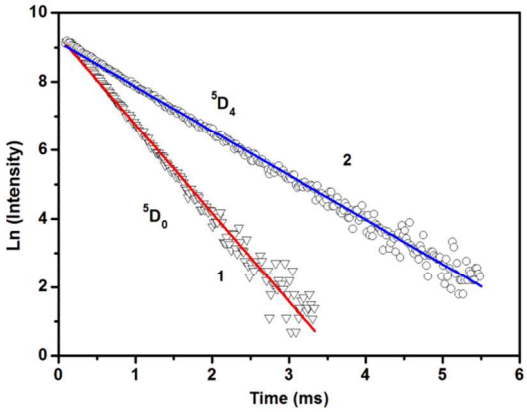

Fig. 14 Room temperature emission decay curves of compound **1** excited at 284 nm and monitored at 617 nm and of compound **2** excited at 288 nm and monitored at 545 nm, respectively.

The room-temperature $^5D_0(Eu^{3+})$ and $^5D_4(Tb^{3+})$ luminescence decay curves were recorded by exciting at the maximum emission wavelengths of $^5D_0 \rightarrow {}^7F_2$ (compound **1**, 617 nm; compound **6**, 615 nm) and $^5D_4 \rightarrow {}^7F_5$ (compounds **2** and **7**, 545 nm) transitions for compounds **1**, **6** and **2**, **7**, respectively. As shown in Fig. 14 and Fig. 15, the luminescence decay curves of compounds **1**, **2**, **6** and **7** fit well into single-exponential functions. The lifetime values (τ_{obs}) of compounds **1**, **2**, **6** and **7** were determined as 0.46 ms, 0.83 ms, 0.69 ms and 0.89 ms, respectively.

The overall quantum yield (Φ_{tot}) is calculated from sensitization efficiencies (η_{sens}) and the intrinsic quantum yield (Φ_{Ln}) of the lanthanide luminescence according to the reported formula[37] $\Phi_{tot} = \eta_{sens}\Phi_{Ln}$. Φ_{Ln} can be calculated by τ_{obs} and natural lifetime (τ_R)[38] using the formula $\Phi_{Ln} = \tau_{obs}/\tau_R$ and $1/\tau_R = A_{MD,0}n^3(I_{tot}/I_{MD})$, where $A_{MD,0}$ = 14.65 s^{-1} which stands for the odds of spontaneous radiative transition of $^5D_0 \rightarrow {}^7F_1$, n is the refractive index of medium, I_{tot} is the sum of Eu^{3+} emission spectrum peak area integral, while I_{MD} is the area integral of

magnetic dipole transition peak area ($^5D_0 \rightarrow {}^7F_1$).[39] Radiative lifetimes (τ_R), intrinsic quantum yields of the lanthanide

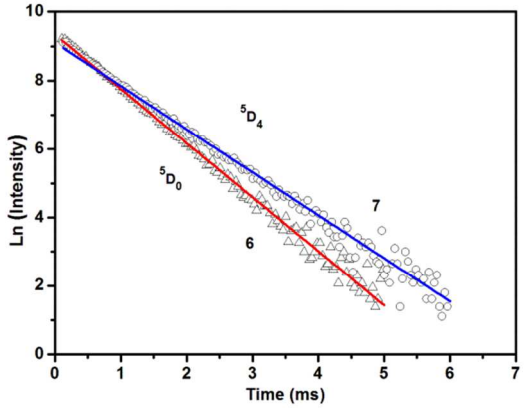

Fig. 15 Room temperature emission decay carves of compounds **6** and **7** excited at 315 nm and monitored at 619 nm and excited at 320 nm and monitored at 545 nm, respectively.

luminescence (Φ_{Ln}), sensitization efficiencies (η_{sens}), the experimentally determined luminescence lifetimes (τ_{obs}) and overall quantum yields (Φ_{tot}) of compounds **1**, **2**, **6** and **7** are listed in Table 3. It can be found that the overall quantum yields (Φ_{tot}) of compounds **1**, **2**, **6** and **7** are low which may be caused by the coordination of the water molecules with Ln^{3+} ions. Both luminescence lifetimes (τ_{obs}) and overall quantum yields (Φ_{tot}) of compounds **6** and **7** are larger than that of compounds **1** and **2**, which is mainly due to more NNO^- ligands and less water molecules coordinated with Ln^{3+} ions existed in compounds **6** and **7** than that in compounds **1** and **2**. On the other hand, the experimentally determined luminescence lifetimes (τ_{obs}) and overall quantum yields (Φ_{tot}) and sensitization efficiencies (η_{sens}) of compounds **2** and **7** are larger than that of compounds **1** and **6**, which are mainly caused by the more effective energy transfer from the ligands to Tb^{3+} ion in compounds **2** and **7** rather than Eu^{3+} in compounds **1** and **6**, which is consistent with the luminescence spectra analyses above.

Conclusions

In summary, formation of the two series of 3-D Ln-MOFs with the formula $[Ln_2(NNO)_2(OX)_2(H_2O)_4]_n$ and $[Ln_2(NNO)_4(OX)(H_2O)_2]_n$ based on HNNO and H_2OX under same hydrothermal conditions unequivocally demonstrates influence of synthetic factors (herein merely changing molar ratio of reactants) on the structures of the Ln-MOFs. The energy transfer mechanism indicated that the Tb^{3+} luminescence is well sensitized by HNNO and H_2OX ligands, demonstrating efficient energy transfer from the ligands to Tb^{3+} ions, while luminescence of Eu^{3+}, Sm^{3+} and Dy^{3+} ions is difficult to be sensitized by the ligands effectively due to unmatched energy gaps between the triplet state levels of HNNO and H_2OX ligands and $^5D_0$ (Eu^{3+}), $^4G_{5/2}$ (Sm^{3+}) and $F_{9/2}$ (Dy^{3+}). The higher luminescence intensity of compounds **6** - **7** than that of compounds **1** - **2** indicated that the synthetic factors not only impose influence on the structures of the resultant compounds but also affect their luminescence properties. The thermal stability analysis results illustrated that compounds **1** - **10** show remarkable structure stability between 25 ºC - 300 ºC. Compounds **2** and **7** have the advantages of good luminescence and good thermal stability, they are expected to find applications in the luminescent material field.

Acknowledgements

The financial support of the NSFC and PCSIRT (No. IRT1205) and Beijing Engineering Center for Hierarchical Catalysts is greatly acknowledged. Prof. Xue Duan of Beijing University of Chemical Technology is greatly acknowledged for his kind support.

Notes and references

State Key Laboratory of Chemical Resource Engineering, Institute of Science, Beijing University of Chemical Technology, Beijing 100029, P. R. China. E-mail: zhouys@mail.buct.edu.cn; Tel.: +86-10-64414640.

Electronic Supplementary Information (ESI) available: Chart S1, Tables S1 and S2, Figs. S1-S4. See DOI: 10.1039/b000000x/

1 (a)H. L. Guo, Y. Z. Zhu, S. L. Qiu, J. A. Lercher and H. J. Zhang, *Adv. Mater.*, 2010, **22**, 4190-4192; (b) Y. J. Cui, B. L Chen, G. D. Qian, *Coord. Chem. Rev.*, 2014, **273–274**, 76–86; (c) H. M. Peng, H. G. Jin, Z. G. Gu, X. J. Hong, M. F. Wang, H. Y. Jia, S. H. Xu and Y. P. Cai, *Eur. J. Inorg. Chem.*, 2012, **33**, 5562-5570; (d) J. Yang, Q. Yuo, G. D. Li, J. J. Cao, G. H. Li and J. S. Chen, *Inorg. Chem.*, 2006, **45**, 2857-2865;(e) W. M. Liao, H. T. Shi, X. H. Shi and Y. G. Yin, *Dalton Trans.*, 2014, **43**,15305-15307.

2 Y. J. Cui, Y. F. Yue and G. D. Qian, *Chem. Rev.*, 2012, **112**, 1126-1162.

3 K. Binnemans, *Chem. Rev.*, 2009, **109**, 4283-4374.

4 M. A. Camargo, A. Neves, A. J. Bortoluzzi, B. Szpoganicz, F. L. Fischer, H. Terenzi, O. A. Serra, V. G. Santos, B. G. Vaz and M. N. Eberlin, *Inorg. Chem.*, 2010, **49**, 6013-6025.

5 W. T. Chen and S. Fukuzumi, *Inorg. Chem.*, 2009, **48**, 3800-3807.

6 (a) J. Xu, J. Cheng, W. Su and M. Hong, *Cryst. Growth Des.*, 2011, **11**, 2294-2301; (b) X. J. Zhao, R. X. He and Y. F. Li, *Analyst*, 2012, 137, 5190-5192.

7 (a)E. Burkholder, V. C. J. Golub and J. Zubieta, *Inorg. Chem.*, 2003, 42, 6729-6740; (b) X. F. Lv, L. Liu, C. Huang, L. A. Guo, J. Wu, H. W. Hou and Y. T. Fan, *Dalton Trans.*, 2014, **43**, 15475-15481.

8 A. J. Calahorro, D. Fairen-Jimenez, A. Salinas-Castillo, M. E. Lopez-Viseras, A. Rodriguez-Dieguez, *Polyhedron*, 2013, **52**, 315-320.

9 J. Cepeda, R. Balda, G. Beobide, O. Castillo, J. N. Fernández, A. Luque, S. Pérez-Yáñez, P. Román, D. Vallejo-Sánchez, *Inorg. Chem.*, 2011, **50**, 8437-8451.

10 (a) L. J Zhang, D. H. Xu, Y. S. Zhou and F. Jiang, *New J. Chem.*, 2010, **34**, 2470-2478; (b) H. Wang, S. J. Liu, D. Tian, J. M. Jia and T. L. Hu, *Cryst. Growth Des.*, 2012, **12**, 3263-3270.

11 (a) L. N. Jia, L. Hou, L. Wei, X. J. Jing, B. Liu, Y. Y. Wang, Q. Z. Shi, *Cryst. Growth Des.*, 2013, **13**, 1570-1576; (b) H. Wang, S. J. Liu, D. Tian, J. M. Jia, T. L. Hu, *Cryst. Growth Des.*, 2012, **12**, 3263-3270; (c) J. Xiao, B. Y. Liu, G. Wei, X. C. Huang, *Inorg. Chem.*, 2011, **50**, 11032-11038; (d) J. J. Zhang, L. Wojtas, R. W. Larsen, M. Eddaoudi and M. J. Zaworotko, *J. Am. Chem. Soc.*, 2009, **131**,

17040−17041; (e) J. Gu, Z. Gao, Y. Tang, *Cryst. Growth Des.,* 2012, **12**, 3312-3323.
12 V. Derdau, S. Laschat, E. Hupe, W. A. König, I. Dix, P. G. Jones, *Eur. J. Inorg. Chem*., 1999, **6**, 1001-1007.
13 A. Messerschmidt, M. Schneider, R. Huber, *J. Appl. Cryst*, 1990, **23**, 436-439.
14 G. M. Sheldrick, SHELXL-97, Program for the Refinement of Crystal Structure, University of Göttingen, Germany, 1997.
15 S. Q.Su, W.Chen, C. Qin, Z. Y. Song, G. H. Li, X. Z. Song, M. Zhu, S. Wang, Z. M. Hao, H. J. Zhang, *Cryst. Growth Des.*, 2012, **12**, 1808−1815.
16 J. Yang, C. X. Li and J. Lin, *J. Phys. Chem. C*, 2008, **112**, 12777-12785.
17 P. Vojtisek, I. Cisarova and J. Podlaha, *Z. Kristallogr*, 1997, **212**, 226-233.
18 V. W. S. Sheldrick and M. Morr, *Acta Cryst.*, 1981, **37**, 733-734.
19 H. L. Sun, X. L. Wang, L. Jia and W. Cao, *CrystEngComm*, 2012, **14**, 512-518.
20 H. W. Gu, S. X. Xiao, H. Y. Xiao, Y. Xiao, A. T. Li, X. L. Hu and Q. G. Li, *Ind. Eng. Chem. Res.,* 2012, **51**, 4797-4803.
21 G. L. Law, K. L. Wong, Y. Y. Yang, Q. Y. Yi, G. H. Jia and P. A. Tanner, *Inorg. Chem.*, 2007, **46**, 9754-9759.
22 (a) H. Kueppers, F. Liebau, A. L. Spek, *J. Appl. Crystallogr.,* 2006, **39**, 338-346; (b) A. L. Spek, PLATON, A Multi-purpose Crystallographic Tool, Utrecht University, Utrecht, The Netherlands, 2001.
23 (a) G. V. Girichev, N. I. Giricheva, A. Haaland, N. P. Kuzmina, S. Samdal, T. N. Strenalyuk, N. V. Tverdova and I. G. Zaitseva, *Inorg. Chem*. 2006, **45**, 5179-5186; (b) W. G. Lu, D. C. Zhong, L. Jiang and T. B. Lu, *Cryst. Growth Des.,* 2012, **12**, 3675-3683.
24 (a) F. J. Steemers, W. Verboom and D. N. Reinhoudt, *J. Am. Chem. Soc*., 1995, **117**, 9408-9414; (b) M. V. Lucky, S. Sivakumar and M. L. P. Reddy, *Cryst. Growth Des.,* 2011, **11**, 857-864; (c) P. C. R. Soares-Santos, L. Cunha-Silva and H. I. S. Nogueira, *Cryst. Growth Des.,* 2008, **8**, 2505-2516.
25 W. X. Feng, Z. Zhang and X. Q. Lv, *Inorg. Chem.,* 2012, **51**, 11377-11386.
26 L. F. Marques, S. M. V. dos, S. J. L. Ribeiro, E. E. Castellano, F. C. Machado, *Polyhedron,* 2012, **38**, 149-156.
27 P. C. R. Soares-Santos, L. Cunha-Silva, F. A. Almeida Paz, R. A. S. Ferreira, J. Rocha, L. D. Carlos and H. I. S. Nogueira, *Inorg. Chem.,* 2010, **49**, 3428-3440.
28 L. J. Zhang, S. Xu, Y. S. Zhou, *CrystEngComm*, 2011, **13**, 6511-6519.
29 P. Wang, R. Q. Fan, X. R. Liu, *CrystEngComm*, 2013, **15**, 1931-1949.
30 M. Kleinerman, *J. Chem. Phys*., 1969, **51**, 2370-2381.
31 Y. L. Gai, F. L. Jiang, L. Chen, M. Y. Wu, K. Z. Su, J. Pan, X. Y. Wan and M. C. Hong, *Cryst. Growth Des*. 2014, **14**, 1010-1017.
32 (a) X. L. Tang, W. Dou, S. W. Chen, F. F. Dang and W. S. Liu, *Spectrochim. Acta, Part A*. 2007, **68**, 349−353; (b) N. Arnaud, E. Vaquer and J. Georges, *Analyst,* 1998, **123**, 261-265; (c) T. M. Reineke, M. Eddaoudi, M. Fehr, D. Kelley and O. M. Yaghi, *J. Am. Chem. Soc.,* 1999, **121**, 1651-1657.
33 (a) F. S. Richardson, *Chem. Rev.,* 1982, **82**, 541–552; (b) S. Surble, C. Serre, F.Millange, F. Pelle and G. Ferey, *Solid State Sci.,* 2007, **9**, 131-136.
34 D. T. Lill, A. Bettencourt-Dias, C. L. Cahill, *Inorg. Chem.*, 2007, **46**, 3960-3965.
35 (a) X. Y. Chen and G. K. Liu, *J. Solid State Chem.*, 2005, **178**, 419–428; (b) Q. Ju, Y. S. Liu, R. F. Li, L. Q. Liu, W. Q. Luo and X. Y. Chen, *J. Phys. Chem. C.* 2009, **113**, 2309–2315.
36 Y. S. Zhou, X. M. Li, L. J. Zhang, Y. Guo and Z. H. Shi, *Inorg. Chem*. 2014, **53**, 3362-3370.
37 C. X. Li, Z. W. Quan, J. Yang, *Inorg. Chem.*, 2007, **46**, 6329-6337.
38 X. Ma, X. Li and Y. E. Cha, *Cryst. Growth Des.*, 2012, **12**, 5227-5232.
39 M. H. V. Werts, R. T. F. Jukes, J. W. Verhoeven, *Phys. Chem. Chem. Phys*., 2002, **4**, 1542-1548.

Two series of Ln-MOFs of different structures and consequently different chemo-physical properties were obtained by simply controlling the reactants' ratio.